

## CMDs FOR THE LMC CLUSTERS NGC 2249 AND NGC 2241

JOSEPH H. JONES<sup>a)</sup>

Lowell Observatory, Mars Hill Road, 1400 West, Flagstaff, Arizona 86001

Received 27 August 1986; revised 24 April 1987

## ABSTRACT

Color-magnitude diagrams are derived for two LMC clusters, NGC 2249 and NGC 2241. A technique is introduced for "subtracting" the field-star contribution from the cluster CMDs using CMDs from nearby LMC fields. The possibility of a "gap" in the main sequence of NGC 2249 is discussed, and, by identifying the gap as the point of core hydrogen exhaustion for stars with convective cores, the isochrones are found to be well placed relative to the turnoff. Based on these isochrones, NGC 2249 is thought to be  $550$  to  $700 \times 10^6$  years old, depending on the reddening and distance modulus used. NGC 2241, by virtue of its subgiant branch and giant clump and by comparison with NGC 2506, is thought to be between 3 and  $4 \times 10^9$  years old.

## I. INTRODUCTION AND OBSERVATIONS

Star formation in the LMC seems to have had a complex history. The study of LMC cluster CMDs provides a more direct means of unraveling this history. The LMC is also important in determining the distance scale of the universe, and cluster CMDs may help to pin down the LMC distance modulus. Finally, techniques developed to study the LMC clusters from the ground may be applicable to farther members of the Local Group when data from the *HST* become available.

Three LMC clusters were chosen from available photographic data. NGC 2249 was designated the primary cluster of the study, one reason being that integrated colors and magnitudes for this cluster obtained from the literature (van den Bergh 1981; Bernard and Bigay 1974) indicated this cluster to be of intermediate age, between 200 million and 1 billion years old. If the cluster proved to be in the lower part of this range, there was a reasonable chance that the main-sequence (MS) turnoff could be reached with the photographic data and an accurate age determined. This, in turn, would provide one more "calibration point" in the study of integrated light from stellar systems. CCD-derived magnitudes were used as a means to calibrate the photographic magnitudes. The CCD magnitudes were also used to derive a CMD for NGC 2249, although due to adverse observing conditions these data were no deeper than the photographic magnitudes.

Two other clusters were chosen for their proximity to NGC 2249. NGC 2241 and SL 889 are both imaged on the same photographic plates as the primary cluster, so it was possible to calibrate their magnitudes as well using the transformations derived from the primary cluster magnitudes. NGC 2241 is less rich than NGC 2249, but seems almost as concentrated despite its description as an "open" cluster in the revised NGC catalog. SL 889 is a very sparsely populated cluster and may well be a true LMC open cluster. SL 889 will not be considered in this paper, except for a field CMD derived from the outer region of the scanned image of SL 889.

## II. THE CCD DATA: OBSERVATIONS AND REDUCTIONS

The CCD digital images were taken with the Cerro Tololo Inter-American (CTIO) 4 m prime-focus CCD camera by

R. A. Schommer (private communication) on the night of 24 December 1984. An averaged image of three 600 s exposures of NGC 2249 taken through the *V* filter and defringed was chosen for measuring the *V* magnitudes. This image was taken at an airmass of 1.32. A similar file containing the average of three 600 s images taken through the *B* filter was chosen for the *B* magnitude reductions. The airmass of this frame was 1.29. The night was characterized by poor seeing but appeared photometric, so several E-region fields of standard stars were measured (Graham 1982). The seeing on the CCD frames measured about 4 pixels FWHM. With an image scale of 0.6 arcsec per pixel, this is 2.4 arcsec FWHM. This image is shown in Fig. 1 [Plate 22].

To reduce the CCD images of NGC 2249, DAOPHOT was used for PSF fitting. One pass through DAOPHOT's automatic star-finding subroutine turned up over 400 possible stars in the *V* image. The coordinate lists derived from the *V* image were offset to correspond to the *B* image. These coordinates were then used for photometry on the *B* frame.

The instrumental magnitudes from DAOPHOT were normalized to a 1 s exposure and corrected to a large aperture for comparison with the standard stars. Using uncrowded star images on the frames, these corrections were determined to be

$$\Delta v = 0.511 \pm 0.007,$$

$$\Delta b = 0.676 \pm 0.011.$$

DAOPHOT was used to perform aperture photometry on the standards from the Harvard E regions (Graham 1982), and their instrumental magnitudes were used to determine the extinction and color-transformation coefficients.

The resulting value of the visual extinction,

$$k'_v = 0.248 \pm 0.048,$$

is larger than that found over an average of about ten nights by Schommer (1985), but since the standards were observed at approximately the same airmass as the cluster, it was felt that any error would be taken into account in the zero points. The value of the *b* - *v* extinction coefficient was found to be

$$k'_{bv} = 0.095 \pm 0.070.$$

The value of  $k''_{bv}$  used was the value published by Landolt (1983).

The CCD color terms were determined to be

$$\epsilon = -0.026 \pm 0.022, \zeta_v = 0.085 \pm 0.013,$$

$$\mu = 1.090 \pm 0.032, \zeta_{bv} = 0.178 \pm 0.021.$$

<sup>a)</sup> Now at CFHT Corporation, Post Office Box 1597, Kamuela, Hawaii 96743.

The visual color term is in excellent agreement with that found by Schommer (1985). The  $B - V$  color term differs by only 0.052 from his, and this is probably due to the fact that I used a second-order extinction coefficient. The program stars were shifted into the  $BV$  system using these values in the color-transformation equations

$$V = v_0 + \epsilon(B - V) + \zeta_v,$$

$$(B - V) = \mu(b - v)_0 + \zeta_{bv}.$$

The rms scatter of these fits is 0.023 mag in  $V$  and 0.03 mag in  $B - V$ . Using the standard errors of the visual extinction, the aperture correction, and the  $V$  zero point, the total zero-point error in  $V$  is approximately  $\pm 0.06$ . The CCD magnitudes were used as standards to transform the photographic magnitudes into the standard system.

### III. THE PHOTOGRAPHIC DATA: OBSERVATIONS AND REDUCTIONS

The photographic plates were taken with the prime-focus camera on the 4 m telescope at CTIO by Schommer on the night of 2–3 January 1982. The plates were exposed in combination with a Racine wedge so that the brighter standard stars on the plates had secondary images for calibration to deeper magnitudes. Two  $V$  plates and two  $B$  plates were chosen out of several exposures made during the observing run. Exposures of 15 and 25 minutes were chosen in both colors. The seeing was about 1.6 arcsec FWHM on each plate. All plates had 16 calibration spots exposed near the plate edge.

Eight regions containing three clusters and 15 standard stars were scanned on each plate, using the Kitt Peak National Observatory (KPNO) microdensitometer. RICHFLD, a single PSF-fitting program, was used in the crowded frames. In order to use the scanned images, the optical-density measurements were transformed into relative intensity using the program HDCURV. One problem encountered using this program was the way it treated extrapolation beyond the darkest last spot value; very optically dense regions on the plate were not adequately transformed into relative intensity.

Inspection of the images showed that even the dimmest standard stars on the plate had core pixels that were affected by the incomplete transformation into intensity. For this reason, it was necessary to use stars measured in the CCD image as a photoelectric sequence.

Since RICHFLD's PSF-fitting algorithm only fit one star at a time, very crowded stars were not fit as well. No attempt was made to measure extremely crowded stars or stars near the core of the clusters. The scanned photographic fields are shown in Figs. 2–5 [Plates 23–26]. Figures 4 and 5 show the frames used for field stars. Field stars were picked from an annulus around the small cluster SL 889 in Fig. 3, and the lower half of the frame shown in Fig. 5.

### IV. RECALIBRATING THE PHOTOGRAPHIC DATA

Since the photographic images had been transformed into intensity images, it was expected that only a color term and a zero-point difference would be needed to transform the photographic magnitudes into the standard system. Plots of  $V$  (CCD) versus  $V$  (photo) and  $B$  (CCD) versus  $B$  (photo) were checked, and only a few of the brighter  $V$  magnitude stars showed the effects of saturation.

Sixty-two well-fit, uncrowded star images from the CCD image that had also been measured in the photographic image were used like a photoelectric sequence to determine the

color equations between the photographic magnitudes ( $V_p$  and  $B_p$ ) and the CCD magnitudes.

Figure 6 shows the difference between the CCD magnitudes and the photographic magnitudes versus CCD color. The best-fit lines determine the color terms and zero points. The values of these color terms cannot be compared with others derived from similar plates since a rough transformation had already been performed on the photographic magnitudes. The rms scatter is on the order of 0.1 mag, but the number of points used helped to beat down the standard error in the zero point to  $\pm 0.04$ , which would imply a total zero-point error for the photographic magnitudes of approximately  $\pm 0.07$ . This includes the CCD magnitudes' zero-point error.

### V. FINAL MAGNITUDES AND ERROR ESTIMATES

DAOPHOT returns a fitting statistic that is similar to a reduced chi value for the PSF fit. Well-fit star images should cluster around a  $\chi$  of about 1.0 over the whole range of magnitudes. Since the CCD magnitudes were to be used for calibrating the photographic images, only the best-fit images were needed. Therefore, only stars with a  $\chi < 1.5$  were used as CCD program stars. Figure 7 shows the estimated DAOPHOT relative error as a function of magnitude. The CCD  $B$  error is larger because, in terms of instrumental magnitudes, the measurements had to be pushed to fainter limits. The opposite effect occurs for the photographic magnitudes where the  $B$  plates are more sensitive than the  $V$  plates for a given exposure.

RICHFLD also returns an error estimate and a normalized chi-square value for each star measured. However, the normalized chi-square was not used to constrain the photographic data. The photographic program stars had been selected manually and were chosen to be somewhat less crowded. This means there should be less error due to crowding in the photographic data. As Fig. 7 also shows, the photographic error increases rapidly with magnitude. The turnover near the faintest magnitudes is an artifact due to the approximation used to estimate the error. This was noted also by Fahlman, Richer, and VandenBerg (1985).

### VI. ANALYSIS AND SYNTHETIC CLUSTERS

In order to deal with the field-star problem and to facilitate the comparison of the CMDs with the models, gray-level plots of the number density of points on a color-magnitude diagram (ND-CMD) were produced. Given cluster and field magnitudes and colors, and an estimate of the number of field stars in the cluster's CMD, a program calculates the probability that a point on the CMD at a given color and magnitude is a field star. For both the cluster and field CMDs the average number density of points in a uniform array of "positions" (colors and magnitudes) on the CMDs was determined. The points in a region around each position in the array and the estimated error at that position are used to determine the average number density of points for that element in the array. The ND-CMD of field stars is then scaled such that the total number of field stars in the field diagram is the same as the estimated number of field stars in the cluster diagram.

The probability that a point in the cluster CMD is a field star is determined by dividing the number density at a given position on the field CMD by the number density at the same position in the cluster CMD. The following algorithm is used to "clean" the cluster CMD of probable field-star

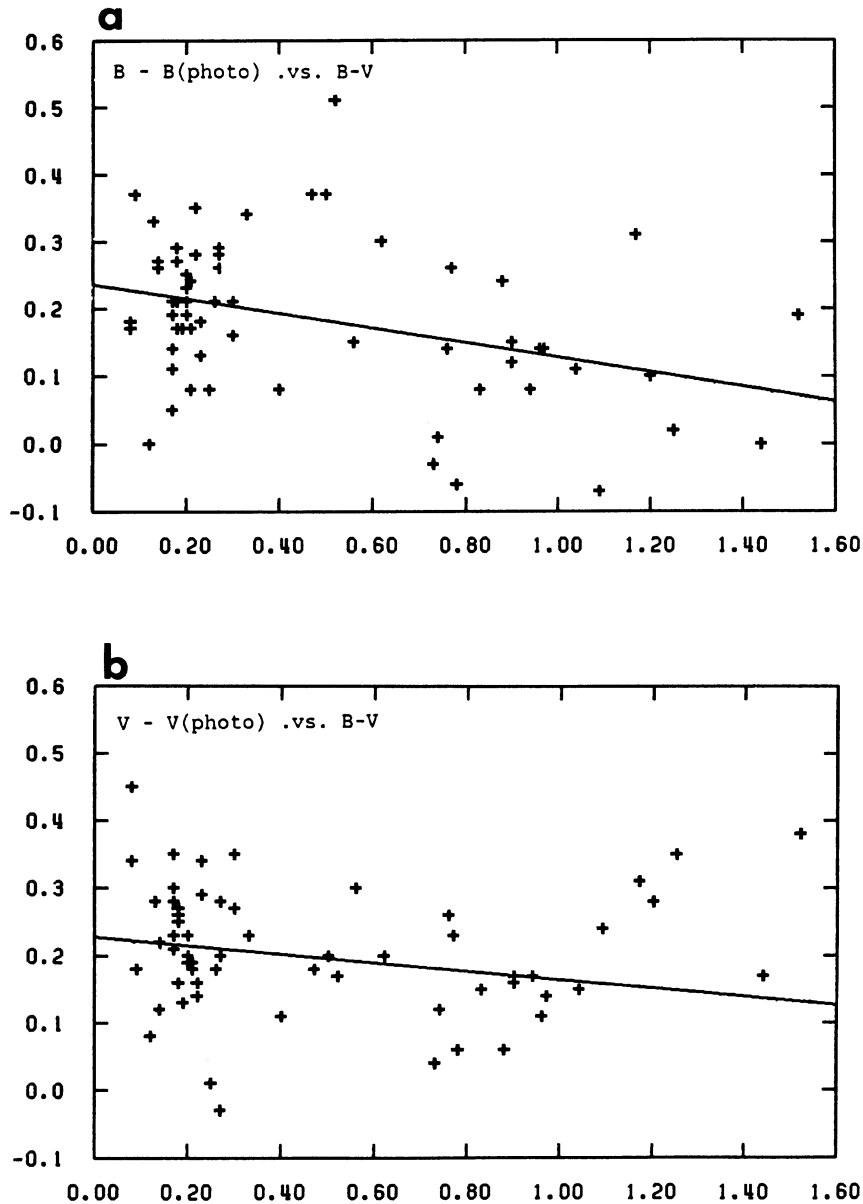


FIG. 6. Color transformation from the photographic magnitudes into the standard system using magnitudes derived from the CCD frame.  $B$  magnitudes (a) and  $V$  magnitudes (b).

points. For each point on the cluster CMD, the program generates a random number between 0 and 1 and checks it against the probability that the point is a field-star point. If it is less than the value of the probability, the point is designated a field star and discarded. The process is repeated three times on the original data, and three cleaned cluster CMDs are generated in order to judge the effects of the random manner in which the field points are deleted. Of course, no information about the individual point is gained; the star measured to determine that point may or may not be a cluster member. However, the major sequences on the CMD as a whole become better defined. The gray-level plots of the ND-CMDs are useful by themselves to some extent. Since the number density at any given point is determined using an average in a region whose size is determined by the error in magnitude and color at that point, features in the CMD that are caused only by the random photometric error tend to be

smoothed out of the ND-CMD. Features such as the major sequences, nonrandom gaps, and significant clumps of points tend to be retained.

The scatter of the observational CMD was evaluated by simulating the effects of random photometric scatter on a realistic CMD derived from model evolutionary tracks. In this project, I have used models derived from the Paczynski code provided by Flower (1985). It is also used to compare the models with the observed diagram. Points taken from evolutionary tracks of different masses were used to interpolate evolutionary tracks for any given stellar mass. Mass points weighted by an initial mass function are randomly chosen, and evolutionary tracks for these masses are interpolated in  $\log(\text{mass})$  between the input tracks. Each mass point is given an age chosen from a Gaussian distribution about some average age to model the star-formation interval. The  $\log(L/L_0)$  and the  $\log(T_{\text{eff}})$  of the mass point are then

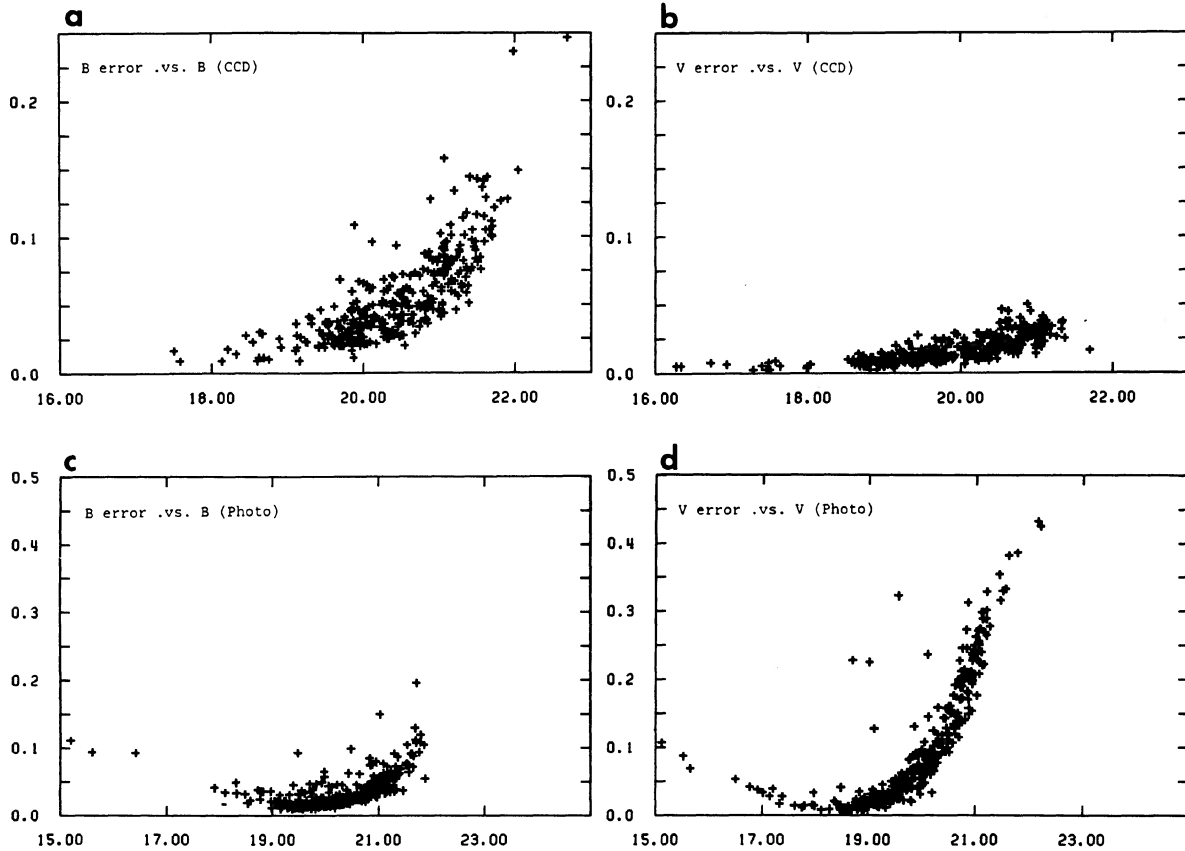


FIG. 7. Relative magnitude error versus magnitude for  $B$  (a) and  $V$  (b) CCD magnitudes and for  $B$  (c) and  $V$  (d) photographic magnitudes.

found from the interpolated evolutionary track and  $V$  magnitudes, and  $B - V$  colors are determined using interpolation tables. The given reddening and distance modulus are then applied to the magnitudes. Finally, using interpolation tables for the standard deviation with magnitude, a Gaussian error spread is added to the magnitudes and colors. The final realistic CMD for this model cluster is plotted with an option for overlaying the isochrone and a zero-age main sequence (ZAMS) for the model.

This procedure is very useful for evaluating the effect of random error on the positioning of the sequences relative to the isochrone and for determining when and if points should show up during certain fast evolutionary periods. By modeling the effects of random photometric error, it is possible to evaluate whether the major spread in the observed CMD is due to some other source, such as crowding or differential reddening.

#### VII. REDDENING AND VISUAL EXTINCTION

In order to complete the analysis of the CMDs, it is necessary to determine the reddening of the cluster starlight. It was not possible to determine the reddening with the available observational data.

Bernard and Bigay (1974) measured the integrated  $UBV$  magnitudes and colors of several LMC clusters. They also determined the interstellar reddening associated with each cluster. They found a reddening value for NGC 2249 of

$$E(B - V) = 0.12 \pm \text{---}$$

Burstein and Heiles (1982), using H I column densities and galaxy counts, estimate the value of the reddening over much of the celestial sphere. In the region of the LMC, they were confined to H I column densities only. The value estimated from the reddening maps was

$$E(B - V) = 0.10 \pm 0.01.$$

Values from Burstein and Heiles (1982) should represent the galactic reddening only, but perhaps in this case it may also include the internal reddening of the LMC. At any rate, we can include values of the internal reddening to determine a maximum reddening value. From de Vaucouleurs (1980b), the internal reddening was found to be

$$E(B - V) = 0.03 \pm 0.01.$$

Since this value added to the galactic reddening is only 0.01 mag greater than the value found by Bernard and Bigay (1974) specifically for NGC 2249, I will take their value of

$$E(B - V) = 0.12 \pm 0.02$$

to be the upper value of the reddening for these clusters. The error is taken from the other determinations of reddening. More recently, Conti, Garmany, and Massey (1986) derive a reddening of

$$E(B - V) = 0.11 \pm \text{---}$$

from early-spectral-type stars in the LMC.

Since these clusters lie well away from the center of the LMC, there may in fact be very little reddening at all, either internally or galactic. As a minimum value for the total red-

dening, I take the value for the foreground reddening found by McNamara and Feltz (1980), which is

$$E(B - V) = 0.034 \pm \text{---}$$

Taking  $R$  (visual extinction per unit reddening) to be the standard value of 3.2, we find the visual extinction to be

$$A_v = 0.38 \pm 0.06$$

for the maximum reddening, and

$$A_v = 0.1 \pm \text{---}$$

for the minimum reddening.

One of the clusters has a well-defined MS, but it stretches only about 1.5 mag. Normally, at least 3 mag of MS are needed before it is safe to use the ZAMS to determine a distance. Therefore, the distance to these clusters must be estimated by other means. The distance to the LMC is well known but, unfortunately, double valued. The long scale of Martin, Warren, and Feast (1979) and Sandage and Tammann (1974) would put the LMC distance modulus at

$$\mu_0 = 18.7 \pm 0.2 .$$

The short scale of de Vaucouleurs (1980b), Eggen (1977), and Schommer, Olszewski, and Aaronson (1984) has

$$\mu_0 = 18.3 \pm 0.1 .$$

On top of this, the LMC is thought to be a relatively flat disk seen almost face-on, but tilted by about  $27^\circ$  to the plane of the sky, with the east side closer. The clusters chosen in this study lie  $5.8^\circ$  east of the LMC centroid. Using the procedure outlined by de Vaucouleurs (1980a), a correction of

$$\Delta\mu = -0.13 \pm 0.04$$

should be made for these clusters if they reside in the disk of the LMC. Given all this, we can set definite limits on the distance moduli of these clusters. If the long scale is correct, then

$$\mu_0 = 18.7 \text{ (or } 18.57 \text{ corrected for tilt) ,}$$

and if the short scale is correct, then

$$\mu_0 = 18.3 \text{ (or } 18.17 \text{ corrected for tilt) .}$$

If we assume the long scale and the large reddening, the

apparent distance-modulus value rises to about 19. This is larger than most estimates; de Vaucouleurs (1980b) gives a value of  $18.6 \pm 0.1$  as the best choice of the apparent distance modulus. This means that, if we assume the long scale, the smaller value of the reddening should be used. This gives an apparent distance modulus in the range of 18.7–18.8. If the reddening for the short scale is taken to be the larger value, then the apparent distance modulus would be in the range 18.6–18.7, almost the same as the long scale. Using the smaller value of the reddening and the short scale gives 18.3–18.4 for the apparent modulus. In summary, we can constrain the values for the apparent distance modulus and reddening to the following choices:

$$\mu = 18.7, \quad E(B - V) = 0.034 ,$$

$$\mu = 18.7, \quad E(B - V) = 0.12 ,$$

$$\mu = 18.3, \quad E(B - V) = 0.034 .$$

### VIII. LMC COMPOSITION

The  $Z$  values of Barbaro (1982) as summarized by Matteucci (1984) range from 0.01 to 0.001. The first value is typical of metallicities found for Cepheids (Feast 1984),

$$[\text{Fe}/\text{H}] = -0.15 .$$

The tips of the MS of both NGC 2249 and NGC 2241 do not suggest they are old enough to contain RR Lyrae stars, no matter which distance scale is used. Therefore, the star clusters studied here probably have metallicities closer to the Cepheids.

The models used for comparison have  $Z = 0.002$  and  $Z = 0.015$  (almost solar). For these  $Z$ , a helium mass fraction of  $Y = 0.25$  is consistent with the abundances found in planetary nebula studies (Dufour 1984).

### IX. NGC 2249 COLOR-MAGNITUDE DIAGRAM

The uncleaned photographic and CCD color-magnitude diagrams are given in Fig. 8. Both CMDs have the same features. A fairly well defined but undersampled MS, starting around  $V = 19.2$ , extends down about 2 mag into a sea of scattered points. Both diagrams show a well-defined clump

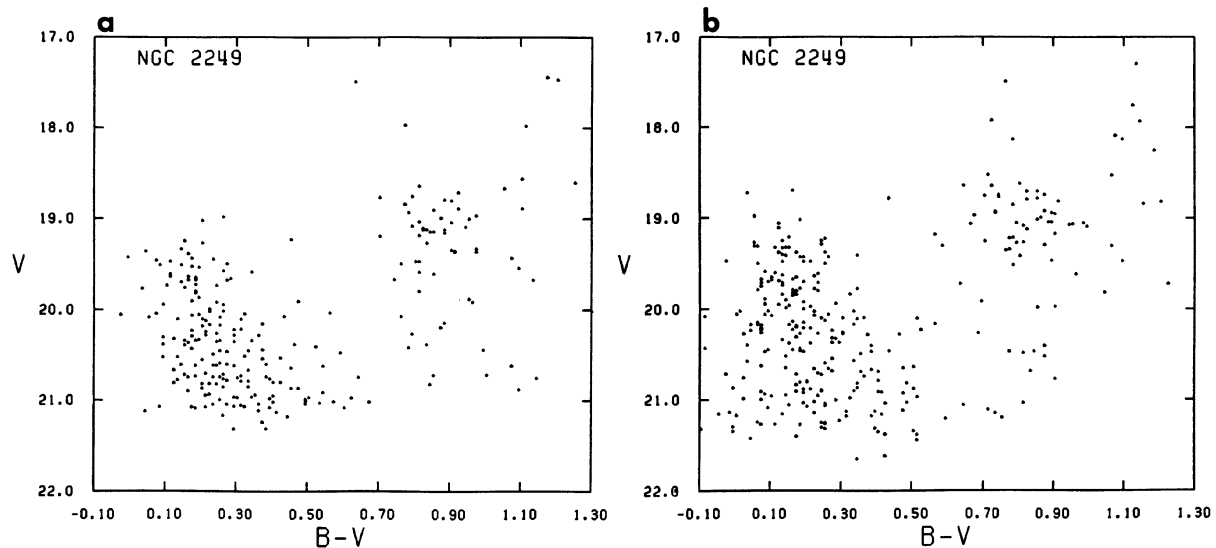


FIG. 8. Original CCD (a) and photographic (b) CMDs for NGC 2249.

of giants at  $V = 18.5\text{--}19.5$  and  $B - V = 0.7\text{--}1.0$  with a hint of a giant branch extending above it. There also seems to be a section of a subgiant branch trailing below the clump. Finally, in addition to the gaps and holes in the body of the MS scatter, there may be a straight gap across the tip of the MS at  $V = 19.5$ . The possible gap is much more apparent in the photographic data, but the same feature seems to show up in the CCD data as well.

The CMDs were cleaned of probable field stars, and ND-CMDs were plotted. These CMDs are shown in Figs. 9 and 10. The field CMD derived from the photographic data was used for both the CCD and photographic cluster CMDs. This CMD is shown in Fig. 14(a). The standard deviation of the smoothing function was derived from the photographic error with magnitude. The MS and giant clump still remain, but the subgiant branch has been eliminated. To lessen the amount of computer time needed to process the diagram, not all of the original diagram was used. The portion of the CMD containing the giant-branch extension has been cut

off, but a few stars still mark where it joins the clump. The lower MS in both CMDs is now even sparser than before, but the upper MS has been less affected. The possible gap near the tip is now slightly more prominent, at least on the photographic CMD. The ND-CMDs show that, at the spot where the gap may be, there is a deep cut in the number density of points between two high-number-density regions. This lends some credence to the possibility of a real feature here.

To test the hypothesis that the gap at the tip is a real feature and not due to random fluctuations, an artificial gap was introduced into the mass function used by the synthetic cluster. More specifically, if any mass point ended up with a  $V$  magnitude between 19.5 and 19.6, it was discarded before any random photometric error was introduced. Figure 11 shows the modeled CMD using the larger photographic error. The gap shows up plainly. Many runs confirm that it also shows up consistently.

There are theoretical reasons to believe that there might be a gap near the tip of the MS, at least for certain mass

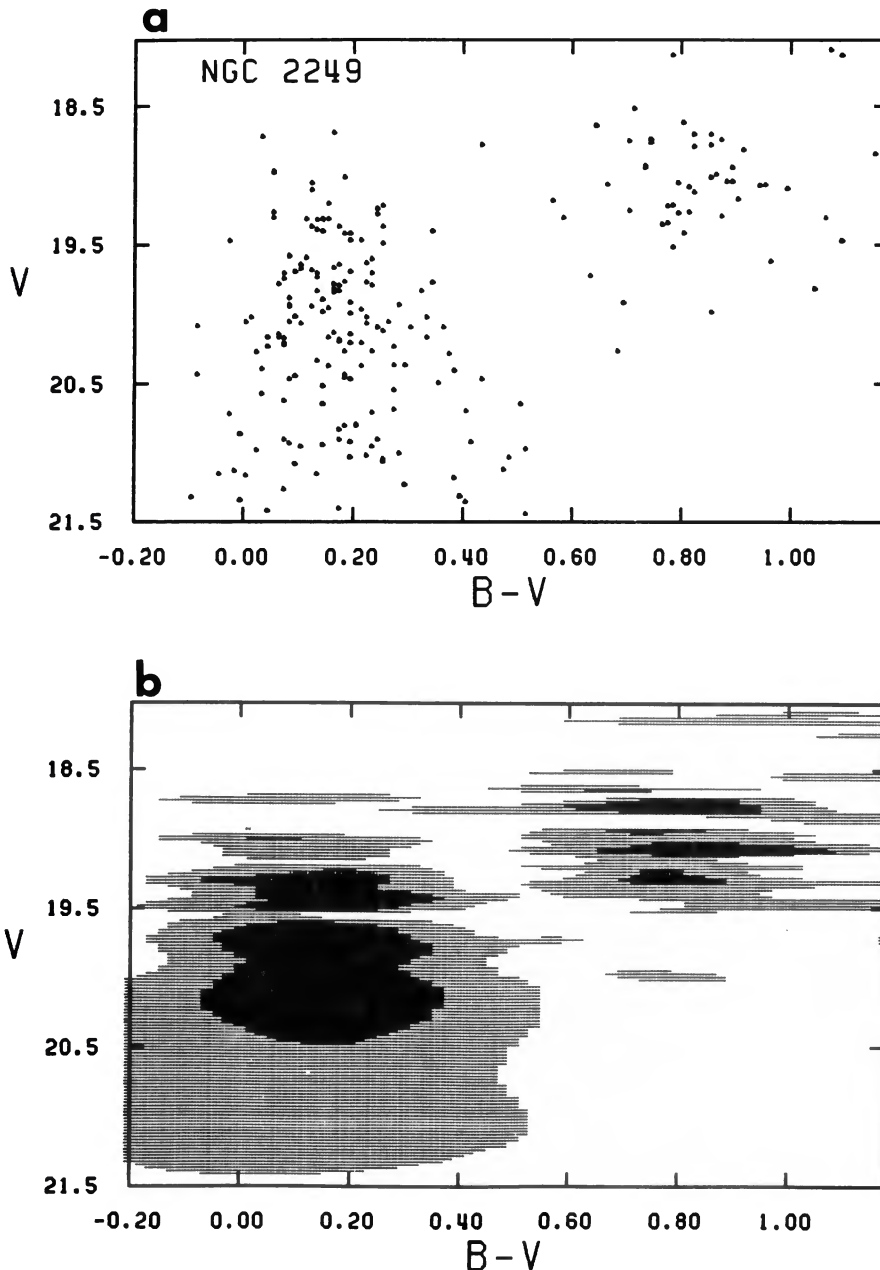


FIG. 9. Photographic CMD with field subtracted (a) and the corresponding number density CMD (ND-CMD) (b) for NGC 2249.

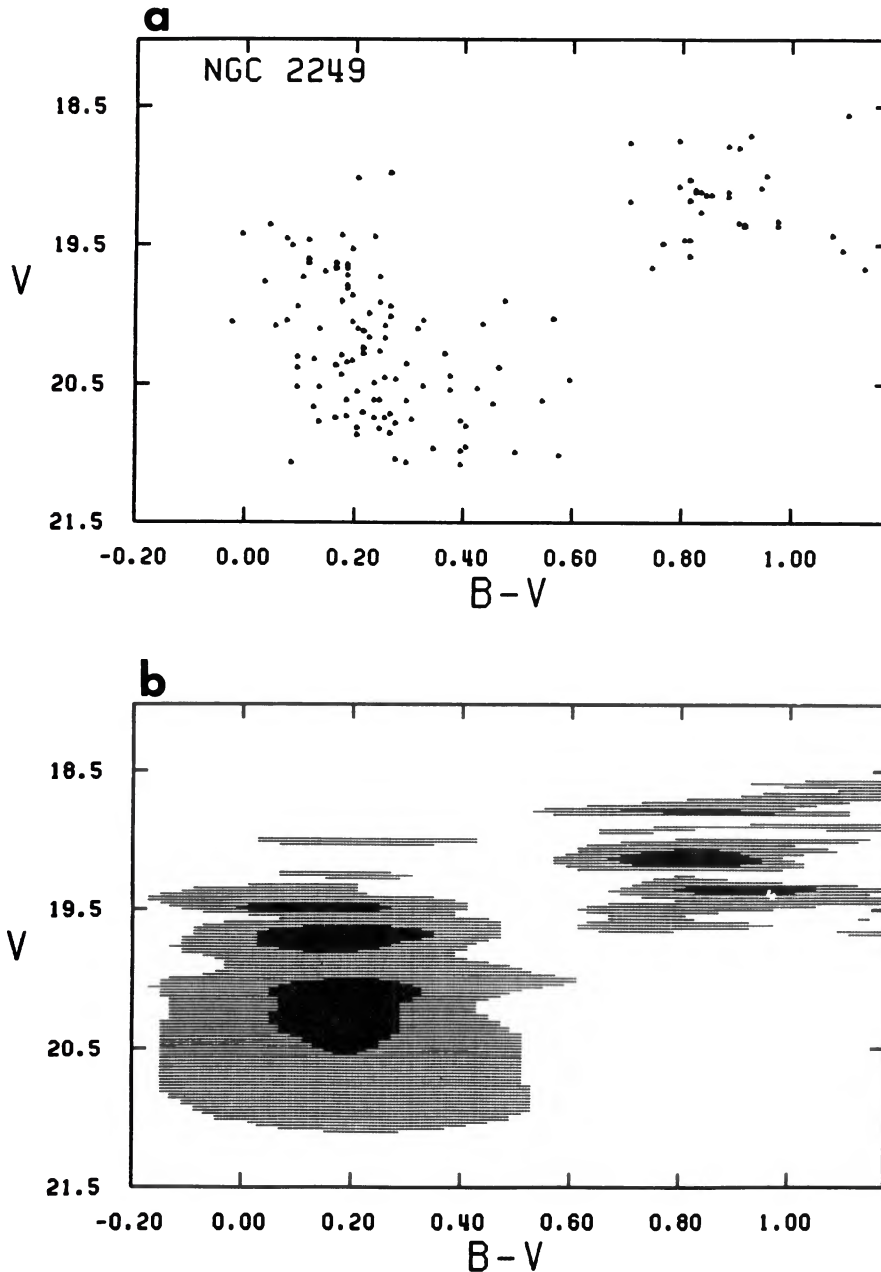


FIG. 10. CCD-derived CMD with field subtracted (a) and the corresponding number density CMD (ND-CMD) (b) for NGC 2249.

ranges. Stellar evolution predicts that, for stars with convective cores, a rapid period of evolution occurs during a phase of overall stellar contraction following the point of core hydrogen exhaustion. The presence of a gap on a CMD would provide a very localized region for comparison with model isochrones.

Gaps in the MS are seen observationally in certain old galactic clusters. Maeder (1974) compares the observed features with the expected features from evolutionary models. He finds that the width in  $V$  magnitude and the “height” above the ZAMS correlates well with the models, but that the number of stars expected in the gap by using a Salpeter (1955) initial mass function is much higher than actually observed. Experiments with the synthetic CMDs show that a gap very seldom appears at the point of hydrogen exhaustion when using the Salpeter mass function, but if a gap in the mass function is artificially introduced, it shows up quite well (Fig. 11). Therefore, if the number of stars in the gap

were reduced, perhaps by a faster evolutionary period than the models indicate, the gap would be visible.

Suppose there is a gap in the data at  $V = 19.5$  in both the CCD and photographic color-magnitude diagrams; identifying this gap as the point of core hydrogen exhaustion, I can then use its position on the observed CMD to match the model isochrones. On following this procedure, the observed turnoff is well placed relative to the isochrone. This means that the conclusions reached using the gap are still valid, even if it is not the point of core hydrogen exhaustion or even if it is not a real feature. Only the claimed accuracy of the match to the isochrone would be in error.

#### X. THE AGE AND DISTANCE MODULUS OF NGC 2249

Models were run using the range of reddenings and distance moduli determined from the literature. For each distance modulus and reddening, a range of isochrones and

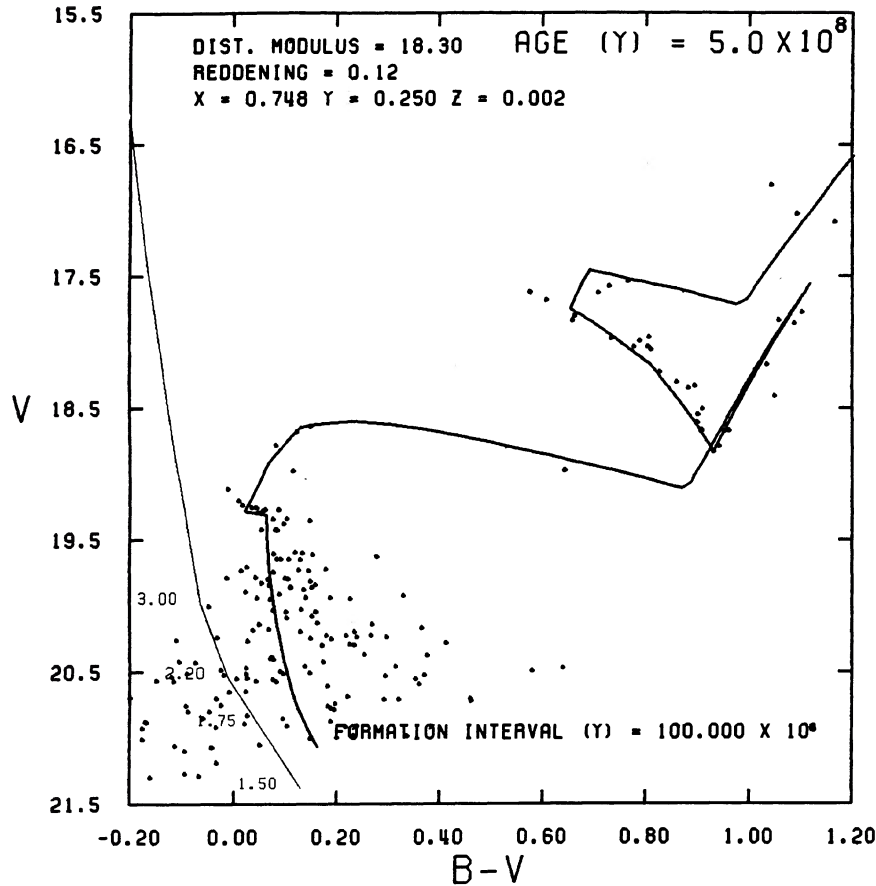


FIG. 11. SYNCLUS-derived CMD using photographic error with modeled gap.

modeled CMDs were output for the two values of  $Z$  considered. Each model CMD was spaced 25 million years from the last, using both the photographic and CCD estimated errors to model the scatter.

On the cleaned CCD color-magnitude diagram a fiducial line representing the best estimated position of the MS was drawn in the following manner. A line was drawn at the base of the supposed gap. Extending from this line, an envelope was drawn on the blue side of the scatter. This represented the extent of the random scatter on the left-hand side of the MS. Using the modeled MS spread as a judge, an envelope was drawn representing the extent of the random scatter on the right-hand side of the MS. Points greater than six times the estimated error from the left line were given low weight. A fiducial line representing the MS was drawn by bisecting lines drawn parallel to the horizontal axis between the envelope of the random scatter. The same procedure was followed using the photographic data. In comparing the photographic fiducial MS against the CCD fiducial MS there was almost a perfect match. The idealized MS was then compared with the isochrones generated by SYNCLUS. I found that, given the distance modulus, the model age could be distinguished to the nearest 25-million-year increment by matching the magnitude of the supposed gap with a line drawn between the points of hydrogen exhaustion on the  $Z = 0.002$  and  $Z = 0.015$  isochrones. Where the fiducial MS line ends up between the two models gives an indication of the composition of the cluster. Remember, if the gap is only a statistical feature, the claimed precision of the comparison with the isochrone is not valid. Table I gives the results for

the three cases considered. Isochrones for these cases are compared to the photographic CMD in Fig. 12.

The colors and luminosities of the giant clump were not well modeled in any of the cases. The lower- $Z$  models tend to model the color of the giants better, while the higher- $Z$  models are closer to the correct magnitude. Therefore, the major weight of the comparison is given to the MS.

Setting the reddening to 0.034 and using the short scale gives a value of 700 million years for the age. The metallicity is between 0.002 and 0.015 but slightly favors the  $Z = 0.015$  isochrone. If the short scale and the higher reddening are assumed, the determined age is about 600 million years old. In this case, the color of the MS indicates a metallicity between 0.002 and 0.015. Finally, using the long scale with a reddening of 0.034, the best isochrone age is near 550 million years. The color of the fiducial MS is very close to the  $Z = 0.015$  isochrone. Analysis of NGC 2241 later in this paper seems to indicate a reddening closer to the larger value. This might imply the age and distance modulus of NGC

TABLE I. Gap-fitting results for NGC 2249.

$\mu_0$	$E(B-V)$	Age ( $10^9$ )	$Z$
18.3	0.034	700	closer to 0.015
18.3	0.120	600	between 0.002 and 0.015
18.6	0.034	550	very close to 0.015

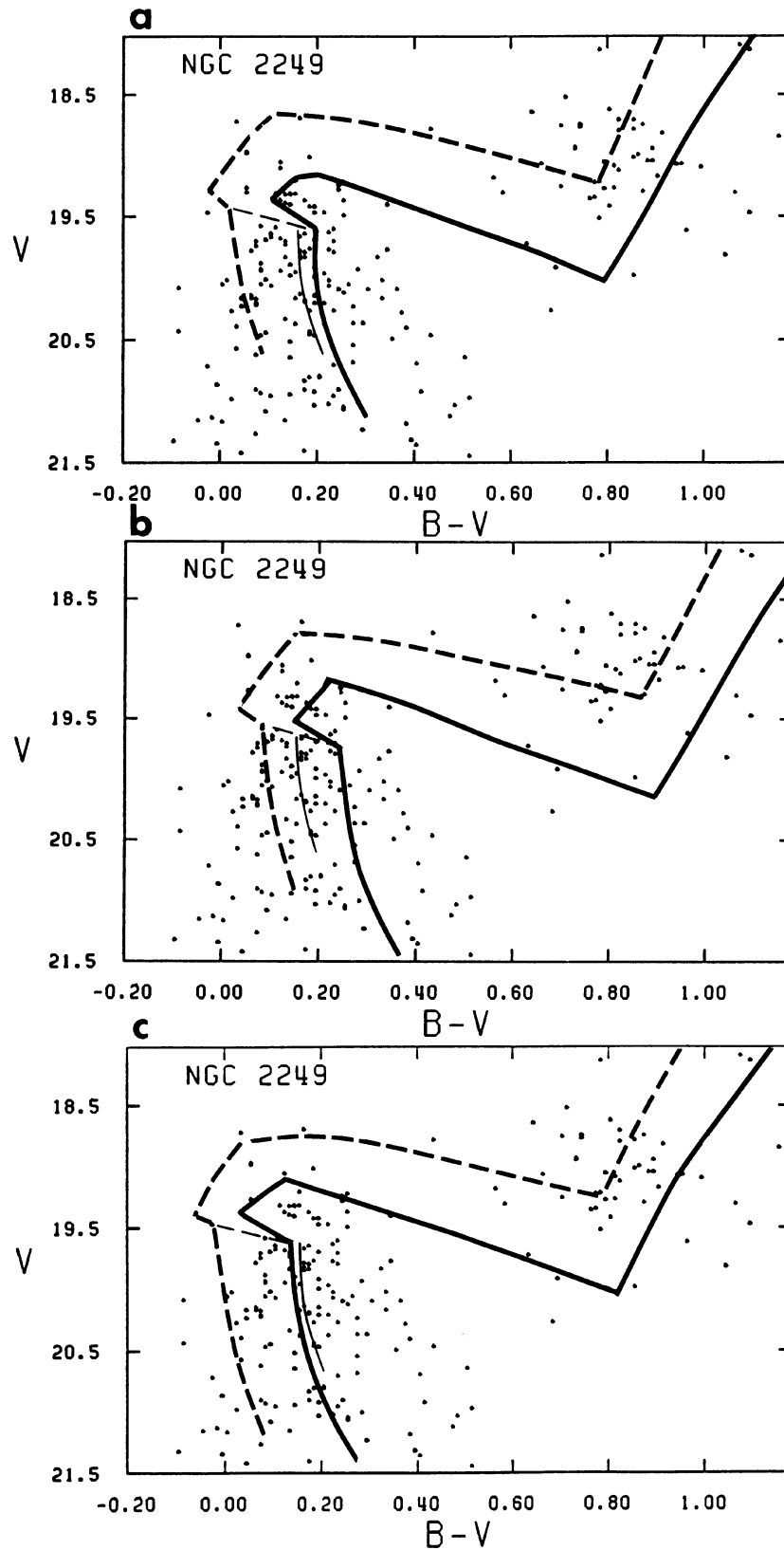


FIG. 12. Cleaned photographic CMDs of NGC 2249 with  $Z = 0.002$  (dashed) and  $Z = 0.015$  (solid) isochrones overlaid. The thin solid line is the fiducial MS. (a) Isochrone age =  $700 \times 10^6$  yr, short scale, low reddening; (b) isochrone age =  $600 \times 10^6$  yr, short scale, high reddening; (c) isochrone age =  $550 \times 10^6$  yr, long scale, low reddening.

2249 to be that for the case with the higher reddening. This case also indicates a metallicity less than solar, which is more in line with the range indicated by the literature.

However, these results depend heavily on the stellar evolutionary models. Other models which incorporate convective overshooting from convective cores burn at higher luminosities and have longer MS lifetimes than classical models (Bertelli, Bressan, and Chiosi 1985). Chiosi and Pigatto (1986) imply that the magnitude at which core hydrogen exhaustion occurs for a  $10^9$ -year-old cluster is on the order of 1 mag brighter than classical models. Thus, if these models are correct, then the long scale would be appropriate for the high reddening if the age is assumed to stay the same. In the three cases above, older isochrones from these new models might be needed in order to fit the observed CMD. Other adjustments to the models could be made, but the point is that the data do not allow a constraint to be placed on the LMC distance modulus even if the reddening were certain.

These newer models are concerned with stars that have convective cores. Since these are the very stars which are thought to be involved with the formation of a gap on the MS, it would be very interesting to model a cluster CMD using isochrones derived from these models to see if gaps occur in the MS. However, better CMDs that clearly show a gap in the MS would be needed for comparison.

#### XI. THE AGE AND DISTANCE MODULUS OF NGC 2241

Figure 13 shows the CMD for NGC 2241 before being cleaned. The best-defined feature is a clump of giants at  $V = 19$  and  $B - V = 1.0$ . Above this is a "spray" of stars and the hint of a weak giant branch. A small group of stars at  $V = 19.7$ ,  $B - V = 0.2-0.3$  lies above the tip of a MS starting

at about 20.2. From the MS tip, there is a large scatter of points down to 21.5 mag. The scatter at this magnitude is consistent with the expected photographic  $B - V$  errors of 0.3 mag. Finally, there is a hint of a subgiant branch running from  $B - V = 0.6-1.0$  at  $V = 20.5$  and then turning upward to the clump.

Field stars were subtracted from this CMD. The field near NGC 2249 was used first, and then a field derived from the outer region of the image of the small cluster SL 889 was used. This field CMD is shown in Fig. 14(b). This field was closer; therefore it was felt that it might more nearly represent the field population around NGC 2241. However, it also contained some member stars from SL 889, so there was a danger of cleaning the diagram too thoroughly. At any rate, both fields produced similarly cleaned CMDs. Figure 15 shows the cleaned diagram using the field near NGC 2249. The clump of giants at  $V = 19$  is still well defined. Using the other field, the clump is still there, but weaker. This is probably due to using a field contaminated with cluster giants from SL 889. The group of stars above the MS tip is now reduced in number using either field. Most importantly, the loose subgiant branch is still most definitely there. Unlike NGC 2249, it was not subtracted out by either field. This suggests that NGC 2241 is probably greater than  $10^9$  years old. In the models that I used, the oldest usable isochrone in the  $Z = 0.002$  model was at about  $1.5 \times 10^9$  yr. Using either distance scale, this modeled MS tip was still well above the observed one.

Two metal-poor galactic cluster CMDs were found in the literature and compared with NGC 2241. Table II gives the metallicities, ages, reddenings, and distance moduli of the clusters. Figure 15 also shows the schematic CMDs of these two clusters overlaid on the CMD of NGC 2241 so that their giant clumps are superimposed. Using NGC 2420, a true

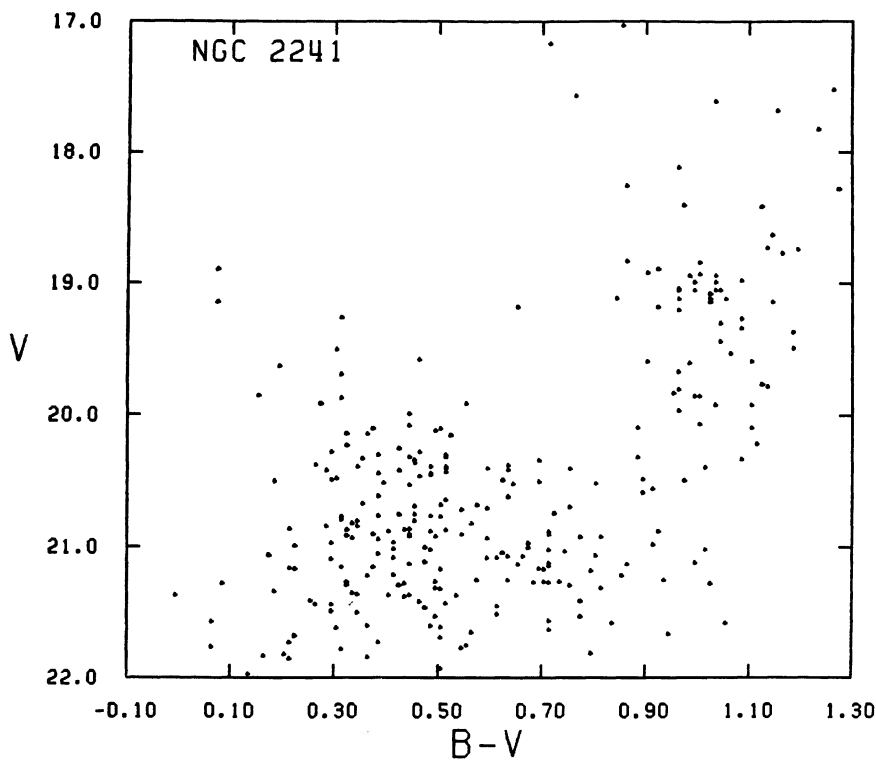


FIG. 13. Original photographic CMD for NGC 2241.

1987AJ.....94...345J

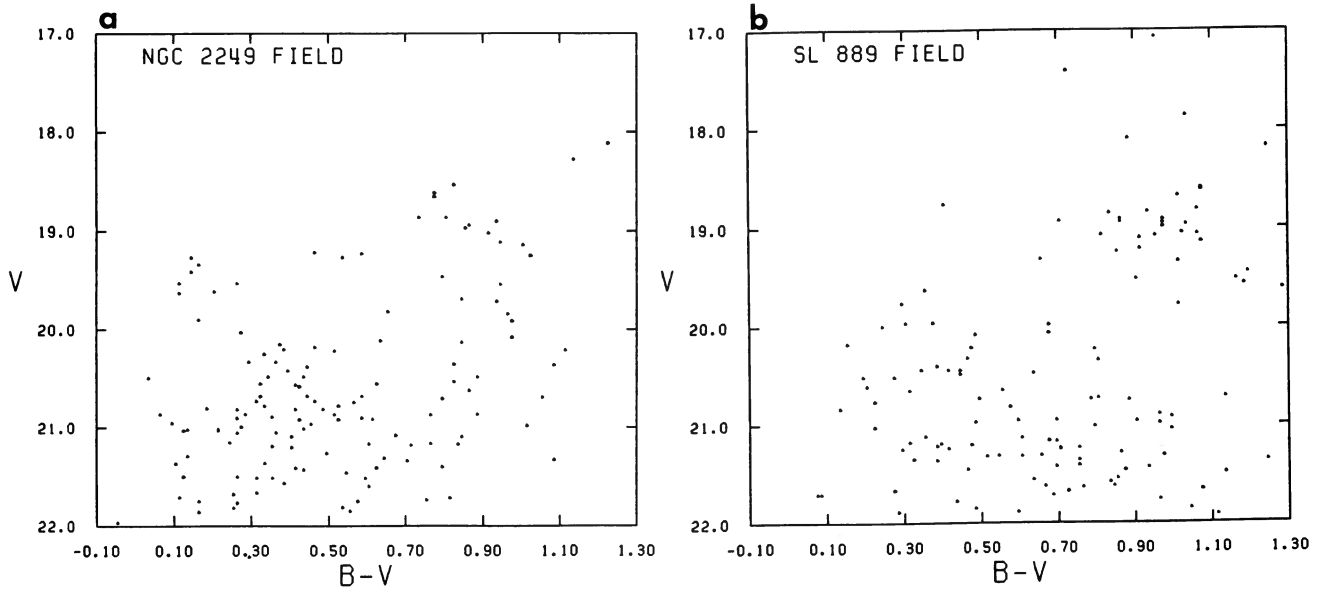


FIG. 14. CMD derived from the photographic field near NGC 2241 (a) and CMD derived from the photographic field around SL 889 (b).

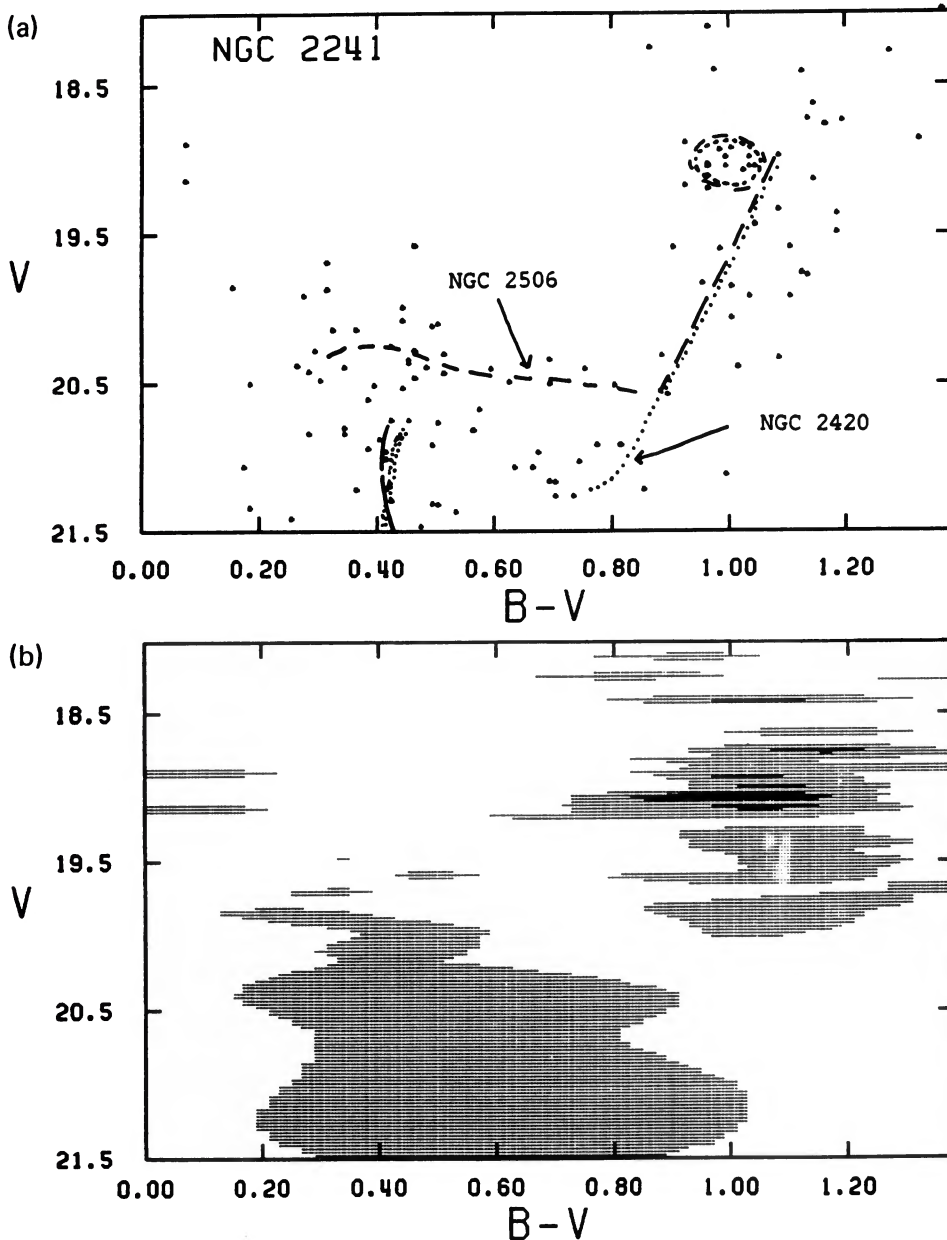


FIG. 15. CMD with field subtracted (a) and the corresponding number density CMD (ND-CMD) (b) for NGC 2241. The fiducial CMDs for NGC 2506 and NGC 2420 are overlaid on the cleaned CMD of NGC 2241 (a).

TABLE II. NGC 2506 and NGC 2420.

Cluster	(v-V) <sub>0</sub>	E(B-V)	[Fe/H]	Age (10 <sup>9</sup> )
NGC 2506 <sup>a</sup>	12.6	0.05	-0.53	4
NGC 2420 <sup>b</sup>	11.8	0.02	-0.34	4

<sup>a</sup>McClure, Newell, and Barnes (1978).

<sup>b</sup>McClure, Twarog, and Forrester (1981).

distance modulus for NGC 2241 of 18.3 is found, with a reddening of 0.01. The subgiant branch seems too faint for a good fit. However, using NGC 2506, a value of 18.4 for the true distance modulus and a reddening of 0.08 are found. This reddening is closer to the maximum reddening that was derived earlier from the literature, and the subgiant branch fits well, which implies a metallicity for NGC 2241 of  $-0.5$  and an age of  $4 \times 10^9$  yr.

## XII. SUMMARY

Based on the models used in this paper, NGC 2249 is thought to be  $550$  to  $700 \times 10^6$  years old, depending on the reddening and distance modulus used. The reddening estimates returned from analyzing NGC 2241 and the fields imply the higher reddening. This in turn implies an age of  $600 \times 10^6$  yr and the short scale, but models with convective overshooting of central convective cores suggest the long scale and the possibility of an older age. With the data at hand it is not possible to choose between distance scales. The composition is implied to be slightly metal poor relative to the Sun, if the higher reddening is used. If the lower reddening is used, the isochrone metallicity that seems to fit is closer to solar metallicity.

NGC 2241, by virtue of its subgiant branch and giant clump and by comparison with NGC 2506, is thought to be between  $3$  and  $4 \times 10^9$  years old. A reddening of 0.08 and a true distance modulus of 18.4 are implied.

The presence of a gap at the point of core hydrogen exhaustion could increase the precision by which observations of clusters could be compared to evolutionary models. However, the detection of the gap is very subjective in these data and cannot be confirmed. A more thorough study of NGC 2249 could be carried out with deeper photometry to decrease the random photometry errors and increase the possibility of detecting the gap in the MS.

Finally, the technique of using CCD photometry to establish a standard sequence on a photographic plate could prove useful by combining the wide-field capabilities of the plate with the linear photometric advantages of the CCD.

This project began at Clemson University as a Ph.D. dissertation. I would like to thank Phil Flower and Robert Schommer for providing the initial guidance and the observational data for this work. Also, thanks to Jeanette Barnes and Ed Carter at KPNO for their help with RICHFLD and the PDS in the reduction of the photographic data and to Peter Stetson for providing a version of DAOPHOT for the data reduction done at Clemson. Hugh Harris at USNOFS and Bill Baum at Lowell provided many helpful insights for which I am very grateful. I appreciate an anonymous referee's comments, which proved to be very useful and helped direct the final revisions. Thanks also to Helen Horstman for the text processing and to Stuart Jones for help with the figures. Finally, I appreciate the support and encouragement from my wife Tori during this project.

## REFERENCES

- Barbaro, G. (1982). *Astrophys. Space Sci.* **83**, 143.  
 Bernard, A., and Bigay, J. H. (1974). *Astron. Astrophys.* **33**, 123.  
 Bertelli, G., Bressan, A., and Chiosi, C. (1985). *Astron. Astrophys.* **150**, 33.  
 Burstein, D., and Heiles, C. (1982). *Astron. J.* **87**, 1165.  
 Chiosi, C., and Pigatto, L. (1986). *Astrophys. J.* **308**, 1.  
 Conti, P. S., Garmany, C. D., and Massey, P. (1986). *Astron. J.* **92**, 48.  
 de Vaucouleurs, G. (1980a). *Publ. Astron. Soc. Pac.* **92**, 576.  
 de Vaucouleurs, G. (1980b). *Publ. Astron. Soc. Pac.* **92**, 579.  
 Dufour, R. T. (1984). In *Structure and Evolution of the Magellanic Clouds*, IAU Symposium No. 108, edited by S. van den Bergh and K. S. de Boer (Reidel, Boston), p. 353.  
 Eggen, O. J. (1977). *Astrophys. J. Suppl.* **34**, 1.  
 Fahlman, G. G., Richer, H. B., and Vandenberg, D. A. (1985). *Astrophys. J. Suppl.* **58**, 225.  
 Feast, M. W. (1984). In *Structure and Evolution of the Magellanic Clouds*, IAU Symposium No. 108, edited by S. van den Bergh and K. S. de Boer (Reidel, Boston), p. 154.  
 Flower, P. J. (1985). Private communication.  
 Graham, J. A. (1982). *Publ. Astron. Soc. Pac.* **94**, 244.  
 Landolt, A. U. (1983). *Astron. J.* **88**, 439.  
 Maeder, A. (1974). *Astron. Astrophys.* **32**, 177.  
 Martin, W. L., Warren, P. R., and Feast, M. W. (1979). *Mon. Not. R. Astron. Soc.* **188**, 139.  
 Matteucci, F. (1984). In *Structure and Evolution of the Magellanic Clouds*, IAU Symposium No. 108, edited by S. van den Bergh and K. S. de Boer (Reidel, Boston), p. 95.  
 McClure, R. D., Newell, B., and Barnes, J. V. (1978). *Publ. Astron. Soc. Pac.* **90**, 170.  
 McClure, R. D., Twarog, B. A., and Forrester, W. T. (1981). *Astrophys. J.* **243**, 841.  
 McNamara, D. H., and Feltz, K. A. (1980). *Publ. Astron. Soc. Pac.* **92**, 587.  
 Mihalas, D., and Binney, J. (1981). *Galactic Astronomy* (Freeman, San Francisco), p. 24.  
 Salpeter, E. E. (1955). *Astrophys. J.* **121**, 161.  
 Sandage, A. (1970). *Astrophys. J.* **162**, 841.  
 Sandage, A., and Tammann, G. A. (1974). *Astrophys. J.* **190**, 525.  
 Schommer, R. A., Olszewski, E. W., and Aaronson, M. (1984). *Astrophys. J. Lett.* **285**, L53.  
 Stetson, P. B., Vandenberg, D. A., and McClure, R. D. (1985). *Publ. Astron. Soc. Pac.* **97**, 908.  
 van den Bergh, S. (1981). *Astron. Astrophys. Suppl.* **46**, 79.

# NGC 2249

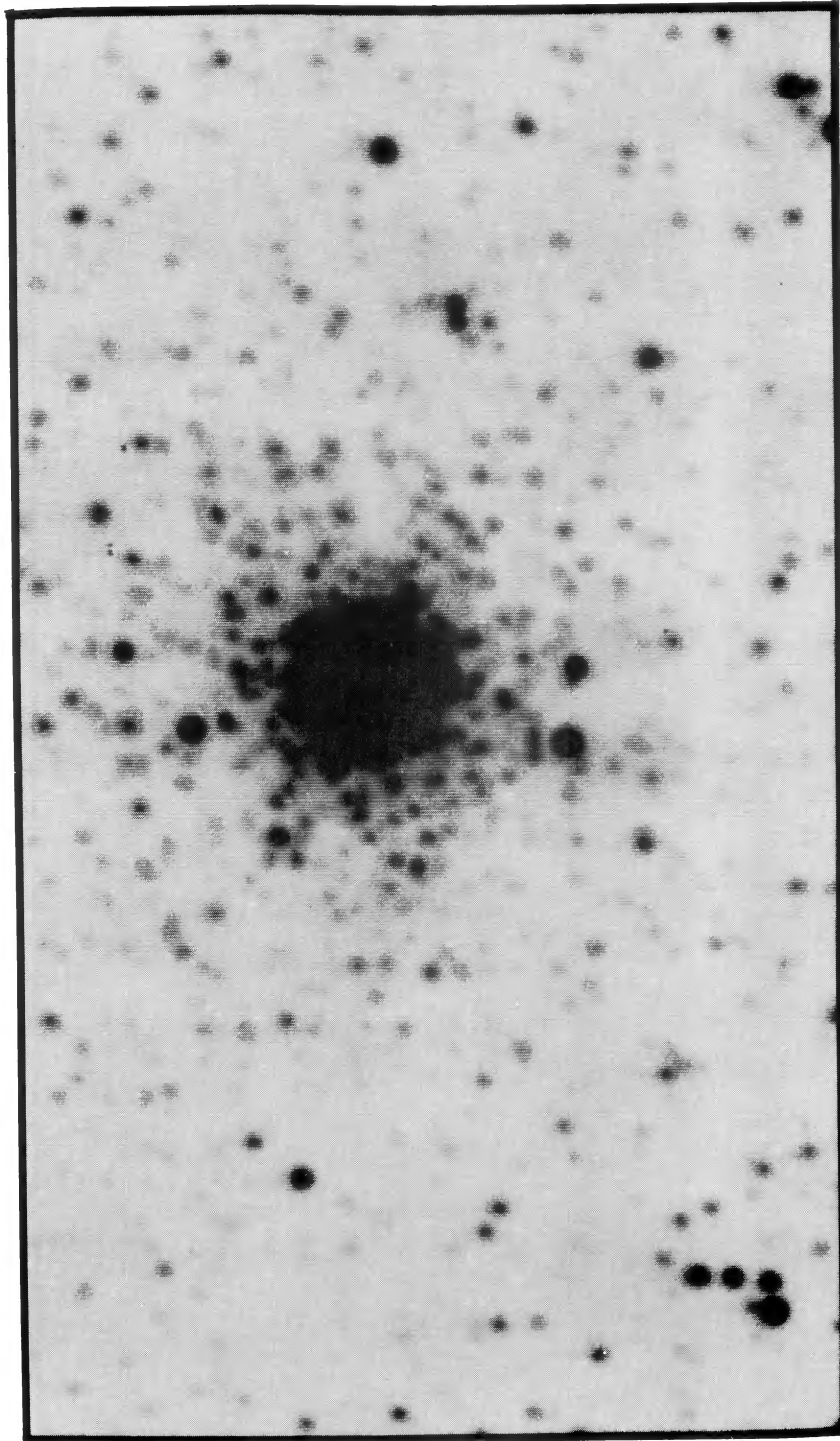


FIG. 1. CCD frame of NGC 2249.

Joseph H. Jones (see page 345)

# NGC 2249

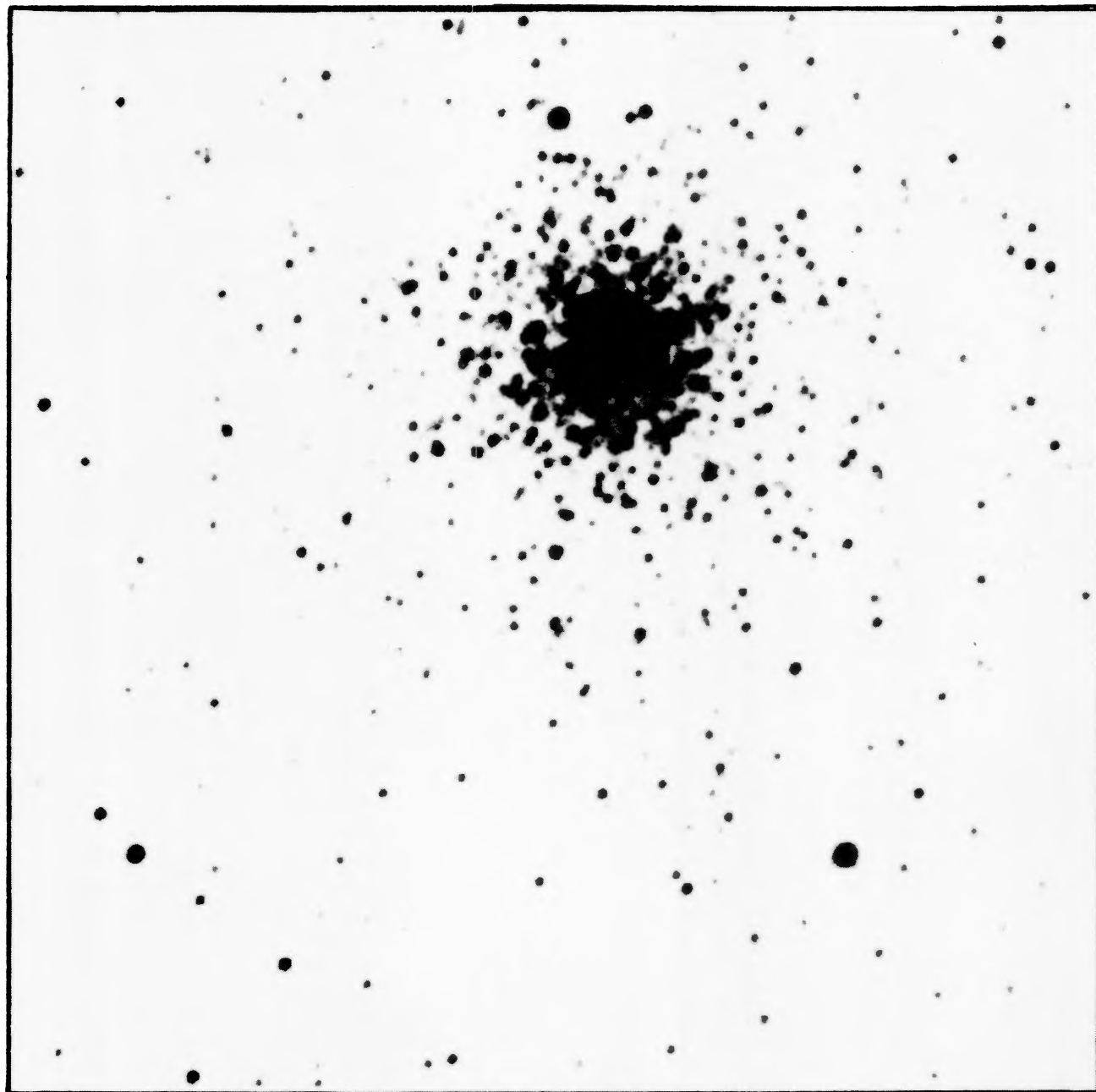


FIG. 2. NGC 2249.

Joseph H. Jones (see page 346)

1987AJ.....94..345J

# NGC 2241

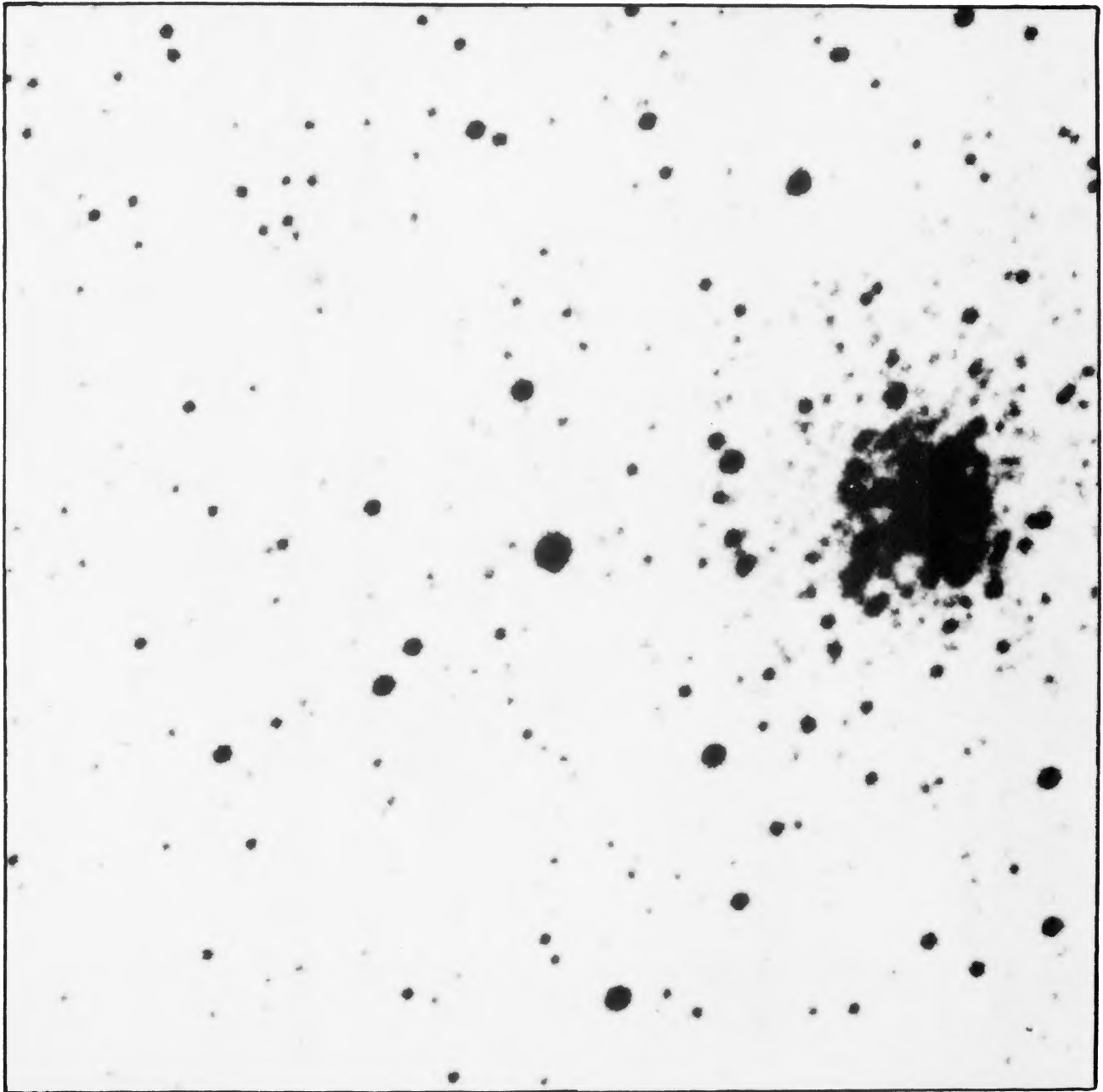


FIG. 3. NGC 2241.

Joseph H. Jones (see page 346)

SL 889

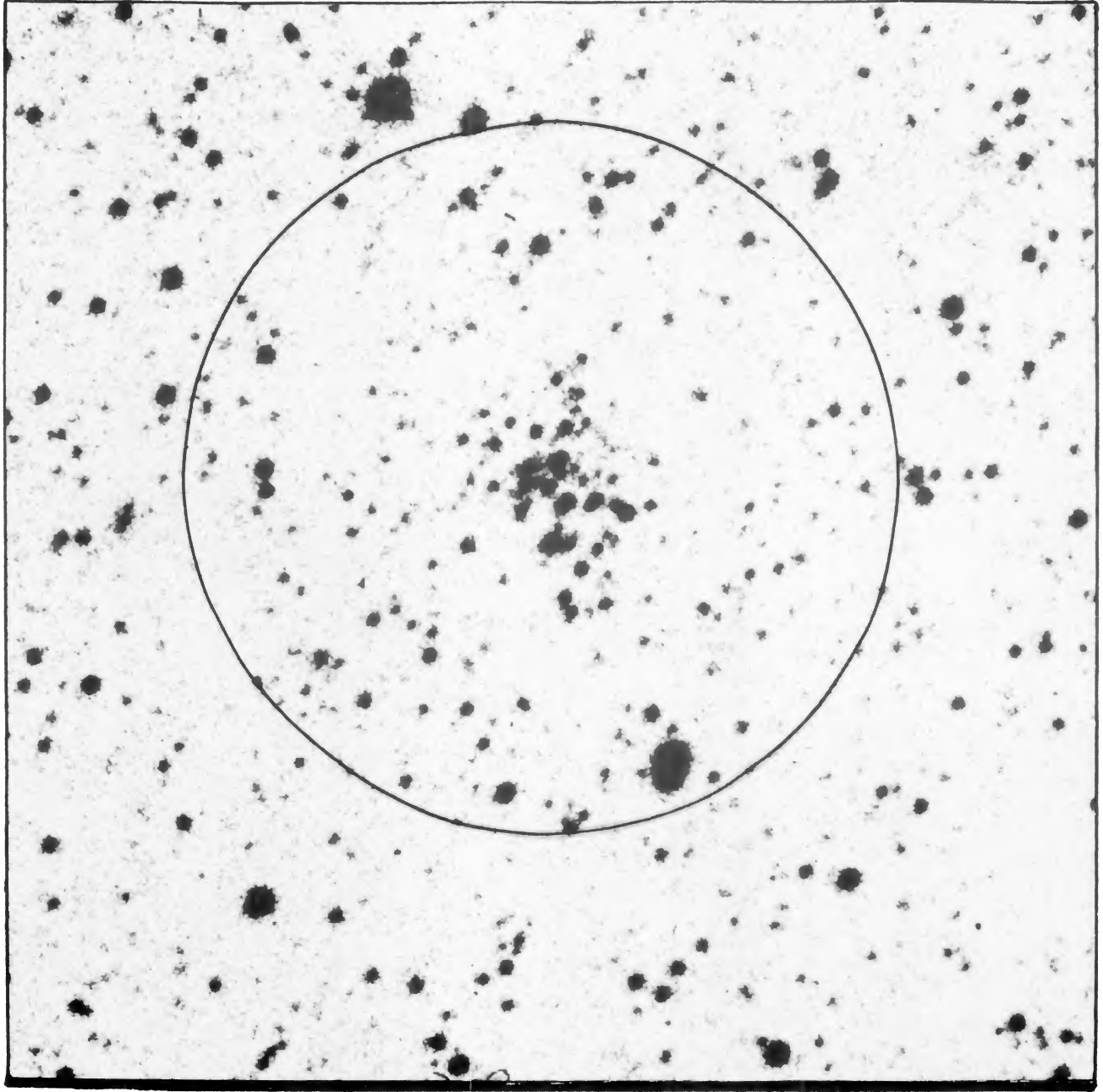


FIG. 4. SL 889; stars outside the annulus were used as field stars.

Joseph H. Jones (see page 346)

## NGC 2249 FIELD

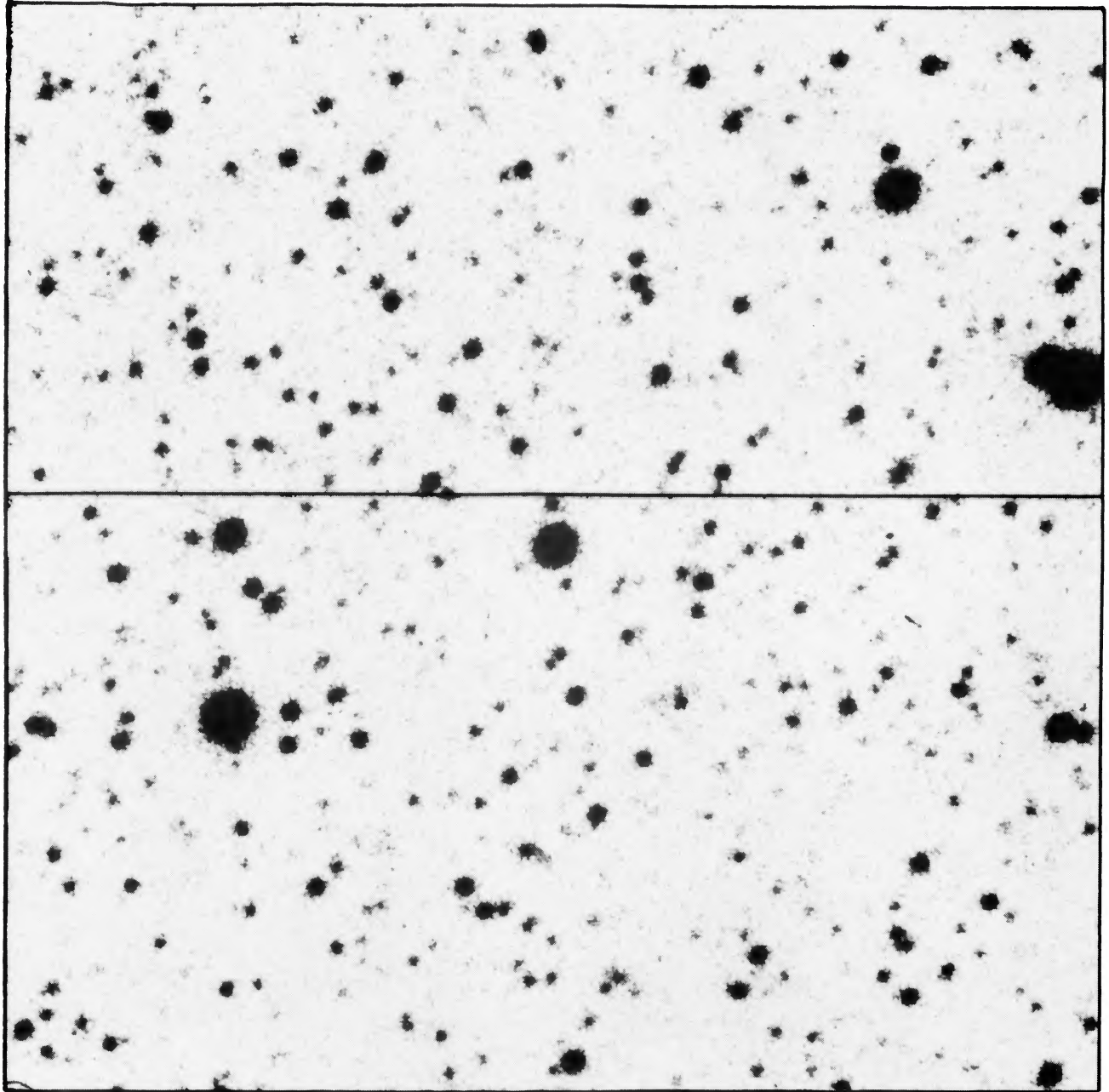


FIG. 5. Field near NGC 2249; only the lower half of the frame was used.

Joseph H. Jones (see page 346)